Soft Matter

Trapping bond exchange phenomenon revealed for off-stoichiometry cross-linking of phase-separated vitrimer-like materials

Journal:	*Soft Matter*
Manuscript ID	SM-ART-01-2024-000074.R1
Article Type:	Paper
Date Submitted by the Author:	29-Feb-2024
Complete List of Authors:	Kito, Takumi; Nagoya Institute of Technology Hayashi, Mikihiro; Nagoya Institute of Technology; PRESTO, Japan Science and Technology Agency

ARTICLE

Trapping bond exchange phenomenon revealed for off-stoichiometry cross-linking of phase-separated vitrimer-like materials

Received 00th January 20xx,
Accepted 00th January 20xx

DOI: 10.1039/x0xx00000x

Takumi Kito,[a] Mikihiro Hayashi *[a,b]

Vitrimer materials combined with nano-phase separated structure have attained attention, which expands the tuning range of physical properties, such as flow and creep properties. We recently demonstrated a preparation of vitrimer-like materials with phase-separated nano domains in which the dissociative bond exchange via trans-*N*-alkylation of quaternized pyridine was operated. In this study, we demonstrate a new finding of the bond exchange mechanism, that is, trapping bond exchange phenomenon. The component polymer is a poly(acrylate) containing pyridine side groups randomly along the chain, which is cross-linked by diiodo molecules via pyridine-iodo quaternization, where the quaternized pyridines are aggregated to form nano-size domains. When the cross-linking reaction is performed at the off-stoichiometric pyridine : iodo ratio (i.e., excess of pyridine groups), free pyridine groups are located in the matrix phase. Since the bond exchange in the present system progresses in the inter-domain manner, the dissociated unit bearing pendant iodo is trapped by the free pyridine groups in the matrix, which generates other small aggregates. This trapping phenomenon affects a lot the relaxation and creep properties, which are much different from conventional knowledge of vitrimer physics.

Introduction

Practical thermosets, such as rubbers and epoxy resins, are cross-linked via permanent bonds, exhibiting high thermal, mechanical, and chemical stabilities.[1] On the other hand, there are inevitable difficulties in recycling and healing, which have to be solved to realize sustainable societies. Due to the above background, the concept of covalent adaptable networks (CANs) has attained great attention.[2,3] In this concept, the network structure formed with dynamic covalent bonds (DCBs) is rearranged via the bond exchange, typically by thermal stimulus. The bond exchange provides the sustainable functions, such as recyclability and healability, unlike the practical thermosets.[4,5] Nowadays, DCBs are classified into two groups, that is, dissociative type and associative type.[6,7] For dissociative DCB, the bond exchange passes through distinct separated steps of bond dissociation and reassociation, whereas for associative DCB, new bond formation occurs before the dissociation of old bond pairs. Particularly, the network materials with a latter type of DCB are termed vitrimers.[8,9]

Generally, any CANs exhibit unique relaxation, creep, and flow properties, which are all owing to the bond exchange reactions in the network.[10,11] Thus, the tuning of bond exchange reaction in the network has been an important issue to regulate the macroscopic properties. So far, effects of various molecular parameters, such as cross-link density and the fraction of bond exchangeable unit, have been studied, revealing that the strand diffusion to find the exchange partner is a key factor to govern the bond exchange.[12-16] As another outstanding strategy, effects of nano-phase separated structure have been explored. [17-21] For example, Sumerlin et al. have prepared diblock copolymer vitrimers; the bond exchange of vinylogous urethane was operated in one block domains in heating,[22] whereas the overall phase-separated structure was maintained during the bond exchange. The results demonstrated that the stress relaxation and creep behaviour were affected by the presence of nano-phase separation. Other examples of nano phase-separated systems were reported for the graft-architecture vitrimers[23] and polyethylene-based vitrimers containing side groups of polyhedral oligomeric silsesquioxane (POSS).[24]

As another simpler type of phase-separated system without complex architectures, we have reported vitrimer-like materials using random copolymers (Figure 1a and 1b).[25] Concretely, the component polymer was a poly(acrylate) bearing pyridine side groups randomly along the chain. The cross-linking relied on the pyridine quaternization reaction with di-halogen molecules, and the reaction progressed quantitatively at the stoichiometric feed ratio of pyridine to halogen groups. Notably, the quaternized pyridine units were aggregated to form small domains at a nm scale, according to the scattering data. The inter-domain dissociative bond exchange via trans-*N*-alkylation was activated in heating without catalysts, which provided the useful sustainable functions.[26] Despite the dissociative bond exchange mechanism, the temperature dependence of relaxation time followed the Arrhenius function, which was a

[a] *Department of Life Science and Applied Chemistry, Graduate School of Engineering, Nagoya Institute of Technology, Gokiso-cho Showa-ku Nagoya-city Aichi Japan, 466-8555*
E-mail: evh70675@ict.nitech.ac.jp
[b] *PRESTO, Japan Science and Technology Agency, 4-1-8, Honcho, Kawaguchi, Saitama 332-0012, Japan*
† Footnotes relating to the title and/or authors should appear here.
Electronic Supplementary Information (ESI) available: [details of any supplementary information available should be included here]. See DOI: 10.1039/x0xx00000x

representative feature of vitrimer-like materials. Based on this molecular design, we have investigated effects of component monomers (i.e., ethyl acrylate or butyl acrylate) and the kinds of halogen cross-linkers (i.e., dibromo or diiodo molecules).

In this study, we newly demonstrate an unusual bond exchange behaviour, that is, trapping bond exchange phenomenon, which eventually affects the relaxation and creep properties. This was found on the system in which the component poly(acrylate) bearing pyridine side groups is cross-linked via diiodo molecules at the off-stoichiometry ratio to keep some free pyridine groups in the matrix (see the schematic of molecular designs in Figure 1c). We here prepare two kinds of component polymer with different molecular weights between the pyridine groups (M_{Py}). One has the M_{Py} of 1k, and the other has the M_{Py} of 2k, which are coded as Py-1k and Py-2k, respectively. We then prepare three cross-linked samples using these component polymers. Two samples are prepared using Py-1k at the stoichiometric ratio (i.e., pyridine : iodo = 1: 1) and also at the off-stoichiometric ratio (i.e., pyridine : iodo = 1: 0.5), and these samples are coded as CL-1k-1 and CL-1k-0.5, respectively. The third is prepared using Py-2k at the stoichiometric ratio (i.e., pyridine : iodo = 1: 1), and this sample is coded CL-2k-1. Essentially, a similar cross-link density is attained for CL-1k-0.5 and CL-2k-1, but there are some free pyridine groups as the bond exchange trapping units in the matrix of CL-1k-0.5. Despite the similar cross-link density and the fraction of the bond exchangeable units, the relaxation and creep properties are much different between these two samples, and the comparison with the highest cross-link density sample (CL-1k-1) is discussed. Usually, the relaxation and creep properties are determined by the cross-link density and the fraction of the bond exchangeable units, the result indicates the collapse of the usual rules.

Experimental section

Materials

Acrylate monomers, ethyl acrylate (EA), 4-hydroxybutyl acrylate (4HBA) and other reagents, including triethylamine (TEA), propylamine (PA), phenyl acrylate (PhA), isonicotinoyl chloride hydrochloride (INCH), 1,6-diiodohexane (DIH), were purchased from TCI, Japan. 2-Cyano-2-propyl dodecyl trithiocarbonate used for chain transfer agent (CTA) was purchased from Aldrich. The radical initiator, azobisisobutyronitrile (AIBN), was purchased from Fujifilm Wako Pure Chemical Corporation. EA and 4HBA were purified by passing them through alumina to remove polymerization inhibitors. Other reagents and solvents were used as received.

Preparation of the cross-linked samples

The syntheses of component polymers, Py-1k and Py-2k, were carried out, according to our previous report[25] (see the details in SI, Scheme S1). Three types of cross-linked samples were prepared via the quaternization reaction with the diiodo cross-linker, DIH (please see the feed mole ratio in the result section). For any cases, the polymers and DIH cross-linker were dissolved in THF, and the solutions were mixed in a Teflon-mold. THF was then slowly evaporated at 25° C for 24 h in a heating stage. The dried mixture was heated at 110 °C for 48 h for the cross-linking, resulting in a homogeneous solid film.

Polymer characterization

The dispersity index ($Đ$) and molecular weight were determined by size exclusion chromatography (SEC), using standard series of poly(methyl methacrylate). The set-up used was an LC-20AD pump system, equipped with a RID-20A RI detector (SHIMADZU) and Shodex-gel columns (K-803, K-804, and K-805 (Shodex)). The eluent was DMF containing lithium bromide (0.05 wt%). The elution rate was 1.0 mL/min and the column temperature was 40°C. The unit ratio of acrylate monomers (i.e., EA and 4HBA) in the polymers was estimated using proton nuclear magnetic resonance (^{1}H-NMR) with a Bruker Analytik DPX400 spectrometer (400 MHz). The dimethyl sulfoxide-d_6 was used as the deuterated solvent. The modification of the RAFT residue was investigated via UV-vis spectroscopy using an F-2700 (Hitachi High-Tech).

Spectroscopy

The progress of pyridine quaternization was confirmed using fourier transform infrared spectroscopy (FT-IR). The measurements were performed using an FT-IR 430 spectrometer attached with the ATR set-up (JASCO Co.).

Thermal properties

The glass transition temperatures (T_gs) for the precursor polymers and cross-linked samples were estimated by differential scanning calorimetry (DSC), using a DSC7020 (Hitachi High-Tech). The provided data were obtained during the second heating from −50 °C to 200 °C at a temperature-ramp rate of 10 °C/min. Thermogravimetric analysis (TGA) was conducted for estimation of the decomposition temperature, using a TG/DTA7300 (Hitachi High-Tech). The cross-linked sample was heated from 40 °C to 550 °C at a temperature-ramp rate of 10 °C/min. All the thermal measurements were under N_2 gas flow.

Scattering measurements

The phase-separated structure was assessed by Small-angle X-ray scattering (SAXS) at BL-6A beamlines in the Photon Factory of the High Energy Accelerator Research Organization (KEK) in Tsukuba, Japan. The X-ray wavelength was 1.5 Å and the distance of sample-to-detector was ca. 2000 mm, where the detector was a PILATUS 2M (Dectris Ltd.). The measurements were performed at room temperature (25 °C) and also at 160 °C, using a hot stage (Linkam Scientific Instruments Ltd.). The measurement at high temperature was performed under N_2 gas flow.

Thermo-mechanical properties

The temperature-ramp rheology was conducted to investigate the thermo-mechanical properties of the cross-linked samples, using a uniaxial rheometer Discovery DMA 850 (TA instruments). The strain of 0.1 % was applied and the frequency, f, was fixed to 1 Hz. The sample was heated from -40 °C to 210 °C at a ramp rate of 2 °C/min. All measurements were performed under N_2 gas flow.

Relaxation properties

Stress-relaxation tests were conducted for the cross-linked samples, using a shear-type rheometer MCR302 (Anton Paar) and 8 mm disposable plates. The tests were performed from 130 to 160 °C with an interval of 10 °C, where the applied strain was 5 %. The measurements were performed under N_2 gas flow.

Creep properties

The creep property was investigated by temperature-ramp creep tests, using a TMA7100 (Hitachi High-Tech). The temperature was increased from 100 °C to 200 °C at a ramp rate of 5 °C/min, during which a constant small force (10 kPa) was applied. The tests were performed under N_2 gas flow.

Result

Polymer synthesis and cross-linking reaction

The two kinds of component polymers with different fractions of pyridine groups were synthesized, according to our previous study (see the details in SI, Figure S1-S5).[25] The characterization results of the polymers, including the number average molecular weight (M_n), dispersity index ($Đ$), and the average degree of polymerization for ethyl acrylate units and pyridine side group units (n_{EA} and n_{py}), are summarized in Table 1 (see the estimation protocol of n_{EA} and n_{py} in SI). Note that the two polymers have the similar molecular weights, but different fractions of pyridine units. The average molecular weight between the pyridine groups (M_{Py}), estimated by M_n/n_{py}, was ca. 1k and 2k for the two polymers. The polymers are thus coded Py-1k and Py-2k in the following.

The cross-linking reaction was conducted by reacting the polymer with a diiodo compound via pyridine-iodo quaternization. To demonstrate the present concept, we prepared three cross-linked samples. Two cross-linked samples were obtained using Py-1k at the feed ratio of pyridine : iodo = 1: 1 and also at the off-stoichiometric ratio, i.e., pyridine : iodo = 1: 0.5. These samples are coded as CL-1k-1 and CL-1k-0.5, respectively. The third is prepared using Py-2k at the feed ratio of pyridine : iodo = 1: 1, and this sample is coded CL-2k-1. FT-IR measurements in Figure S6 confirmed the pyridine groups were consumed for quaternization quantitatively for CL-1k-1 and CL-2k-1, whereas there was some fraction of free pyridine groups CL-1k-0.5. Note that the fraction of quaternized pyridine in CL-1k-0.5 was nearly 0.5, according to the comparison of the intensity or area of pyridine signals before and after the reaction, as designed. Therefore, the fraction of quaternized pyridine was the largest for CL-1k-1, and that was similar between CL-1k-0.5 and CL-2k-1 since the fraction of pyridine groups in the precursor Py-2k was half of Py-1k.

The gel fractions estimated by swelling tests for three cross-linked samples were all ca. 100%, despite not all the pyridine groups being reacted in CL-1k-0.5. As thermal characteristics, the T_g values ranged from -11 °C to -3.2 °C, (Figure S7), and the decomposition temperatures, defined at the 5% weight loss in the TGA thermograms (Figure S8), was above 230 °C, regardless of the molecular design.

Scattering analysis

The aggregation of quaternized pyridines was investigated by SAXS. The component polymers did not exhibit distinct scattering (Figure S9), whereas a broad peak appeared after the quaternization reactions (Figure 2). This indicates the nanodomain formation of quaternized pyridines. The scattering data for the cross-linked samples were analyzed based on the Yarusso-Cooper (YC) model.[27] The entire function is written as,

$$\boldsymbol{I(q)} = \boldsymbol{K}\frac{\boldsymbol{V_1^2}}{\boldsymbol{V_p}}\boldsymbol{\Phi(qR_1)^2}\frac{\mathbf{1}}{\mathbf{1}+(\frac{\mathbf{8}\boldsymbol{V_{CA}}}{\boldsymbol{V_p}})\boldsymbol{\Phi}\,(\mathbf{2}\boldsymbol{qR_{CA}})} \quad (1)$$

$$\boldsymbol{V_{CA}} = \frac{\mathbf{4}}{\mathbf{3}}\boldsymbol{\pi R_{CA}^3} \quad (2)$$

$$\boldsymbol{V_1} = \frac{\mathbf{4}}{\mathbf{3}}\boldsymbol{\pi R_1^3} \quad (3)$$

$$\boldsymbol{\Phi(x)} = \mathbf{3}\frac{\boldsymbol{sin\,x - x cos\,x}}{\boldsymbol{x^3}} \quad (4)$$

In this function, the spherical-shaped aggregates with radius R_1 are assumed to be formed and distributed randomly with keeping the radius of closest approach R_{CA} which governs the spatial correlation between neighboring aggregates. The V_P in equation 1 is the average sample volume per aggregate, from which the number density of the aggregates (*ND*) is calculated, and *K* governs the peak amplitude. The experimental spectra are fitted by adjusting the parameters, R_1, R_{CA}, V_P, and *K*. These fitting parameters are represented in Table 2. The value of *d* in Table 2 is the distance between the aggregates, and the calculation was made by $d = 2r\text{-}2R_1$, where the sample volume occupied by an aggregate is assumed to be a sphere having a radius *r*.[28] The values of R_1 were all similar between the samples, whereas the *ND* and *d* were different depending on the fraction of quaternized pyridine groups; a distinctively lower value of *d* was estimated for CL-1k-1, and the values were relatively close between CL-1k-0.5 and CL-2k-1. The difference of *d* is reasonable, because the fraction of quaternized pyridine groups was designed to be the largest for CL-1k-1 and be similar between other two samples.

These results indicate the location of free pyridine groups in the matrix phase for CL-1k-0.5. The domain structure (i.e., the size of aggregates and distance between the aggregates) of CL-1k-0.5 is much different from CL-1k-1, but is rather similar to CL-2k-1. The size of aggregates reflects the number of functional groups in the domain, and thus the numbers of quaternized pyridines in the domain is similar between CL-1k-1 and CL-2k-1, although the number of pyridine group in the precursor polymers (i.e, Py-1k and Py-2k) is different. As the natural consequence, we concluded for CL-1k-0.5 that the free pyridine groups in CL-1k-0.5 were located in the matrix phase.

Relaxation properties

First, the temperature-ramp rheology data is provided in Figure 3. The tanδ peak at ca. 10-30 °C originated from the segmental relaxation, according to the DSC data. The plateau modulus was clearly the highest for CL-1k-1 (5.0MPa) and the values were close between CL-1k-0.5 (1.2 MPa) and CL-2k-1 (0.8 MPa), meaning the cross-link density of CL-1k-1 was much larger than other two samples and that was similar for CL-1k-0.5 and CL-2k-1. The cross-link density calculated from the simple rubber elasticity theory is 5.0×10^{-4} mol/cm^3 for CL-1k-1, 1.2×10^{-4} mol/cm^3 for CL-1k-0.5, and 0.8×10^{-4} mol/cm^3 for CL-2k-1. The largest plateau modulus for CL-1k-1 is consistent with the expectation, because CL-1k-1 possessed the largest fraction of quaternized pyridines and thus exhibited the smallest *d* in the SAXS data. Notably, the reduction of modulus was noticed at ca. 160-170 °C for three samples. The observed modulus

reduction implies the activation of trans-*N*-alkylation bond exchange. The reducing behaviour of the modulus was clearly different among samples; the steepest and shallowest reduction was observed for CL-2k-1 and CL-1k-0.5, respectively, which may originate from the difference of bond exchange manners.

The difference of bond exchange rate was then investigated by stress-relaxation tests. Figure 4 represents the relaxation spectra for three samples at temperatures ranging from 130 to 160 °C. To discuss the relaxation rate difference, the spectra were fitted with the Kohlrausch-Williams-Watts (KWW) function,[29,30] according to equation 5, to estimate the first-order average relaxation time $<\tau>$ on the basis of equation 6 in which Γ represents the gamma function.[31]

$$\frac{\sigma(t)}{\sigma_0} = \exp\left(-\frac{t}{\tau}\right)^{\beta} \quad (5)$$

$$\langle\tau\rangle = \int_0^{\infty} exp\left\{-\left(\frac{t}{\tau}\right)^{\beta}\right\}dt = \frac{\tau \times \Gamma(\frac{1}{\beta})}{\beta} \quad (6)$$

In the equation 5, the τ and β represent the specific relaxation time and the distribution of τ, respectively (see the values of fitting parameters in Table S1). Note that the applicability of the KWW function, instead of simple Maxwell function, indicates the coupling of bond exchange-based relaxation and strand segmental relaxation, as usually demonstrated for vitrimer-like materials.[31] Figure 5 plots the logarithmic values of $<\tau>$ as a function of inverse temperatures (see the values in Table S1). The linear relationship in the plots indicates the Arrhenius dependence of $<\tau>$, i.e., $\tau = \tau_0 \exp(E_a/RT)$ in which E_a represents the activation energy for the bond exchange in the network. The observed Arrhenius dependence confirmed the vitrimer-like nature in these samples. The difference of $<\tau>$, which reflects the bond exchange rate, was obvious in the plots, where $<\tau>$ of CL-1k-0.5 was larger (i.e., slower bond exchange) than CL-1k-1. On the other hand, $<\tau>$ of CL-2k-1 was smaller (i.e., faster bond exchange) than CL-1k-1. The observation of such differences is interesting, considering that the fraction of the quaternized pyridine groups and also the cross-link density was similar between CL-1k-0.5 and CL-2k-1. The E_a values estimated from the Arrhenius dependence were similar (ca. 126 kJ/mol) between the samples.

Discussions

As mentioned in the introduction section, it is generally known that the relaxation time is lowered by decreasing cross-link density,[12-16] which has been interpreted based on the increased diffusion of bond exchangeable units to find exchange partners. The slower relaxation rate of CL-1k-1 than CL-2k-1 can be explained simply by this reasoning, based on the fact that the cross-link density of CL-2k-1 is lower than CL-1k-1. However, the slower relaxation rate for CL-1k-0.5 is unusual, considering the lower cross-link density of CL-1k-0.5 than CL-1k-1. In addition, the fraction of bond exchangeable units for CL-1k-0.5 and CL-2k-1 was close, which provides another question to interpret the difference of relaxation rate between the two samples.

To find some hints for this unusual result, we tentatively performed time-resolved SAXS measurements with heating at 160 °C (Figure 6a). First, the spectra for CL-1k-1 and CL-2k-1 did not change significantly during the heating. On the other hand, for CL-1k-0.5, a shoulder-like small peak gradually appeared in the shorter q region (< 0.3 nm^{-1}) during the heating. It should be reminded that the main scattering peak observed at q ~ 1 nm^{-1} originated from the correlation between the aggregates of quaternized pyridine groups. In fact, a small shoulder is already observed in the spectrum of as-prepared CL-1k-0.5 (see the double-logarithmic SAXS profile at t = 0 min in Figure 6). Thus, for CL-1k-0.5, initially, there are some small aggregates with the correlation distance much larger than the main aggregates. The change of shoulder-peak in Figure 6 indicates the gradual growth of the small aggregates during the bond exchange. It should be again noted here that the bond exchange in the present design is operated with a dissociative pathway of trans-*N*-alkylation, which progresses in the inter-domain manner. In this case, the dissociated unit bearing pendant halogen group has to diffuse through the surrounding matrix to find the exchange partner. If there are free pyridine groups in the matrix (Figure 6b), the dissociated unit could be trapped to form a quaternized bond during the inter-domain exchange. The repeated diffusion of the bond exchange units from the original aggregates and trapping of the dissociated units in the matrix result in the formation and growth of small aggregates with a large correlation distance, which provides the increase in the should-like scattering in the low q region. Notably, the small aggregates formed by the heating at 160 °C were stable at higher temperatures, i.e., 170 °C and 180 °C (Figure S10).

Under the above assumption, the difference of relaxation rate between CL-1k-0.1 and CL-2k-1 can be explained. The relaxation dynamics is known to be dominated by the bond exchange rate in a given system.[32-34] In the present system, the dynamics should be determined by the frequency of inter-domain bond exchange. Thus, if the bond exchange is trapped in the matrix, the relaxation rate is naturally slowed. This may be the probable reason for the slower relation rate of CL-1k-0.5 than CL-2k-1. We also assessed the relaxation behaviors for the sample with a larger fraction of free pyridines using the component polymer Py-1k. The blend ratio of pyridine : iodo was 1 : 0.3, and the cross-linked sample was thus coded CL-1k-0.3. The stress relaxation data indicated that the relaxation time was shorter and thus the relaxation rate was larger for CL-1k-0.3 than CL-1k-0.5 (Figure S11). This order of relaxation rate should be reasoned by the larger diffusivity of network strands in the less cross-linked network, as shown by the difference of relaxation rate between CL-1k-1 and CL-2k-1. Combining this new result, we assume that the relaxation rate is not only determined by the trapping phenomenon, but also by the diffusivity of the network strands. This point will be assessed in more detail by investigating effects of the stoichiometric balance in the broader feed ratio range.

Such a trapping phenomenon actually influenced the creep properties. Figure 7 represents the temperature-ramp creep for CL-1k-0.5 and CL-2k-1, where the Y-axis is the sample length normalized by the length at 100 °C. The linear relationship between the length and temperature was admitted up to ca. 140 °C, whereas there was clear deviation at higher temperatures. This deviation, i.e., creep, is an indication for the activation of the bond exchange, which is known as a representative vitrimer-like property.[10] Although the deviation temperature was similar between two samples, the creep behaviour (i.e., the temperature dependence of the length) at higher temperatures was obviously different. According to the creep studies of vitrimers, the degree of creep is related to the diffusion of the network segments.[35,36] In the present system, the diffusion was

much slower for CL-1k-0.5 than CL-2k-1, judging from the relaxation data. With this regard, the smaller creep for CL-1k-0.5 is understandable. In addition, we conducted temperature-ramp creep tests to check effects of the formation of aggregation by assessing the annealing effects for CL-1k-0.5. Concretely, the tests were performed for the fresh sample (no annealing time) and the sample annealed for 30 min at 160 °C (Figure S12). The annealed sample exhibited slower creep due to the growth of small aggregates in the matrix by the trapped bond exchange units.

So far, there have been a few reports that studied the physical properties of bond exchangeable materials *purposely* at off-stoichiometric cross-linking.[37,38] In the study from Asseche et al. for the network with Diels-Alder bond exchange between furan-maleimide groups,[37] they demonstrated some increase in the strand mobility during the bond exchange when there were more free exchange units (i.e., maleimide group). This is simply due to the cross-link density effect that governs the restriction degree of strand mobility. In the study from Tournilhac and Gresil for transesterification vitrimers,[38] the network was formed by reacting diepoxy molecules and diacyl molecules (= diacid molecules) in the presence of base catalysts, where they conducted systematic studies with varying the feed ratio between epoxy and acyl groups. The results indicated that the epoxy homo-polymerization progressed at the off-stoichiometric ratio, which eventually slowed the relaxation and creep properties. We in this report revealed another finding of off-stoichiometric effects for bond exchangeable materials, based on the phase-separated system for the first time. The unique point in the present system was found in the trapping of bond exchange units in the matrix phase, which eventually affected the relaxation and creep properties. Indeed, for the industrial mass production of polymeric materials, there is a difficulty in adjusting the stoichiometric ratio for the preparation. Therefore, although the observed trapping phenomenon may be specific to the phase-separated systems, accumulation of such knowledge for effects of off-stoichiometry on the macroscopic properties should be meaningful not only in the fundamental sense, but also in the practical sense.

Conclusions

In this study, we demonstrated a trapping phenomenon of bond exchange, based on the design of phase-separated vitrimer-like materials prepared at the off-stoichiometric cross-link condition. In the present system, the pyridines attached in the side groups of poly(acrylate)s were quaternized with diiodo cross-linkers. The quaternized pyridines were aggregated to form main domains, and the inter-domain bond exchange via dissociative trans-*N*-alkylation was activated by heating. When there were free pyridines in the matrix, the delay of relaxation and suppression of creep were observed, which could not be explained by the reported conventional knowledge of cross-link density effects. We attributed these unusual results to the trapping bond exchange phenomenon in which the dissociated unit bearing pendant iodo group was trapped by the free pyridine group in the matrix phase. Recently, the studies of phase-separated vitrimers or vitrimer-like materials have been developing, whereas the matrix chemistry has been disregarded in the reported phase-separated systems. The present knowledge could thus provide some new knowledge on the tuning of bond exchange mechanism and eventually macroscopic function, which is also important in the viewpoint of practical application.

Author Contributions

Takumi Kito: data curation, formal analysis, investigation, validation, writing – original draft
Mikihiro Hayashi: formal analysis, methodology, project administration, supervision, validation, visualization, writing – original draft, writing – review & editing

Conflicts of interest

There are no conflicts to declare.

Acknowledgements

We thank Prof. K. Nagata for his assistance in performing TGA. The SAXS measurements were performed in beamline BL-6A at the Photon Factory (PF) of the High Energy Accelerator Research Organization in Tsukuba, Japan (KEK). The temperature-ramp rheology measurements were supported by Mr. Y. Otsuka in TA Instruments, Inc. This work was supported by JST, PRESTO Grant Number JPMJPR23N7, Japan.

References

1 P. C. Himenz and T. P. Lodge, Polymer Chemistry; 2nd ed; CRC PRESS, 2007.
2 R. J. Wojtecki, M. A. Meador and S. J. Rowan, *Nat. Mater.*, 2011, **10**, 14-27.
3 M. Podgórski, B. D. Fairbanks, B. E. Kirkpatrick, M. McBride, A. Martinez, A. Dobson, N. J. Bongiardina and C. N. Bowman, *Adv. Mater.*, 2020, **32**, 1906876.
4 X. X. Chen, M. A. Dam, K. Ono, A. Mal, H. B. Shen, S. R. Nutt, K. Sheran and F. Wudl, *Science*, 2002, **295**, 1698-1702.
5 H. Otsuka, *Polym. J.*, 2013, **45**, 879-891.
6 G. M. Scheutz, J. J. Lessard, M. B. Sims and B. S. Sumerlin, *J. Am. Chem. Soc.*, 2019, **141**, 16181-16196.
7 M. Hayashi, *Polymers*, 2020, **12**, 1322.
8 W. Denissen, J. M. Winne and F. E. Du Prez, *Chem. Sci.*, 2016, **7**, 30-38.
9 M. Guerre, C. Taplan, J. M. Winne and F. E. Du Prez, *Chem. Sci.*, 2020, **11**, 4855-4870.
10 D. Montarnal, M. Capelot, F. Tournilhac and L. Leibler, *Science*, 2011, **334**, 965-968.
11 A. Jourdain, R. Asbai, A. Omaima, M. M. Chehimi, E. Drockenmuller and D. Montarnal, *Macromolecules*, 2020, **53**, 1884-1900.
12 L. Yang, L. J. Li, L. H. Fu, B. F. Lin, Y. Q. Wang and C. H. Xu, *Polym. Chem.*, 2022, **13**, 6650-6661.
13 Q. Li, S. Q. Ma, P. Y. Li, B. B. Wang, H. Z. Feng, N. Lu, S. Wang, Y. L. Liu, X. W. Xu and J. Zhu, *Macromolecules*, 2021, **54**, 1742-1753.
14 M. Hayashi, *ACS Appl. Polym. Mater.*, 2020, **2**, 5365-5370.
15 T. Isogai and M. Hayashi, *Macromolecules*, 2022, **55**, 6661-6670.
16 T. Isogai and M. Hayashi, *Polym. Chem*., 2024, **15**, 269-275.

17 B. J. Zhao, L. Li, J. W. Hu, H. M. Wang, H. G. Mei and S. X. Zheng, *Polymer*, 2022, **242**, 124591.
18 S. Weerathaworn and V. Abetz, *Macromol. Chem. Phys.*, 2023, **224**, 2200248.
19 H. G. Fang, X. C. Gao, F. Zhang, W. J. Zhou, G. B. Qi, K. Song, S. Cheng, Y. S. Ding and H. H. Winter, *Macromolecules*, 2022, **55**, 10900-10911.
20 M. Hayashi and L. Chen, *Polym. Chem.*, 2020, **11**, 1713-1719.
21 M. Hayashi, H. Obara and Y. Miwa, *Mol. Syst. Des. Eng.*, 2021, **6**, 234-241.
22 J. J. Lessard, G. M. Scheutz, S. H. Sung, K. A. Lantz, T. H. Epps and B. S. Sumerlin, *J. Am. Chem. Soc.*, 2020, **142**, 283-289.
23 R. G. Ricarte, F. Tournilhac, M. Cloître and L. Leibler, *Macromolecules*, 2020, **53**, 1852-1866.
24 B. Zhao, G. Hang, L. Li and S. Zheng, *Mater. Today Chem.*, 2022, **24**, 100759.
25 Y. Oba, T. Kimura, M. Hayashi and K. Yamamoto, *Macromolecules*, 2022, **55**, 1771-1782.
26 M. Hayashi, Y. Oba, T. Kimura and A. Takasu, *Polym. J.*, 2021, **53**, 835-840.
27 D. J. Yarusso and S. L. Cooper, *Polymer*, 1985, **26**, 371-378.
28 Y. Miwa, J. Kurachi, Y. Sugino, T. Udagawa and S. Kutsumizu, *Soft Matter*, 2020, **16**, 3384-3394.
29 T. Kimura and M. Hayashi, *J. Mater. Chem. A.*, 2022, **10**, 17406-17414.
30 K. Yamawake and M. Hayashi, *Polym. Chem.*, 2023, **14**, 680-686.X
31 M. Hayashi, *Nihon Reoroji Gakkaishi*, 2022, **50**, 15-20.
32 F. L. Meng, M. O. Saed and E. M. Terentjev, *Nat. Commun.*, 2022, **13**, 5753.
33 J. S. Xia, J. A. Kalow and M. O. de la Cruz, *Macromolecules*, 2023, **56**, 8080-8093.
34 Y. G. Sun, K. W. Wan, W. H. Shen, J. X. He, T. Zhou, H. Wang, H. Yang and X. H. Shi, *Macromolecules*, 2023, **56**, 9003-9013.
35 A. M. Hubbard, Y. X. Ren, C. R. Picu, A. Sarvestani, D. Konkolewicz, A. K. Roy, V. Varshney and D. Nepal, *ACS Appl. Polym. Mater.*, 2022, **4**, 4254-4263.
36 A. M. Hubbard, Y. X. Ren, D. Konkolewicz, A. Sarvestani, C. R. Picu, G. S. Kedziora, A. Roy, V. Varshney and D. Nepal, *Acs Applied Polymer Materials*, 2021, **3**, 1756-1766.
37 S. Terryn, J. Brancart, E. Roels, R. Verhelle, A. Safaei, A. Cuvellier, B. Vanderborght and G. Van Assche, *Macromolecules*, 2022, **55**, 5497-5513.
38 Q. A. Poutrel, J. J. Blaker, C. Soutis, F. Tournilhac and M. Gresil, *Polym. Chem.*, 2020, **11**, 5327-5338.

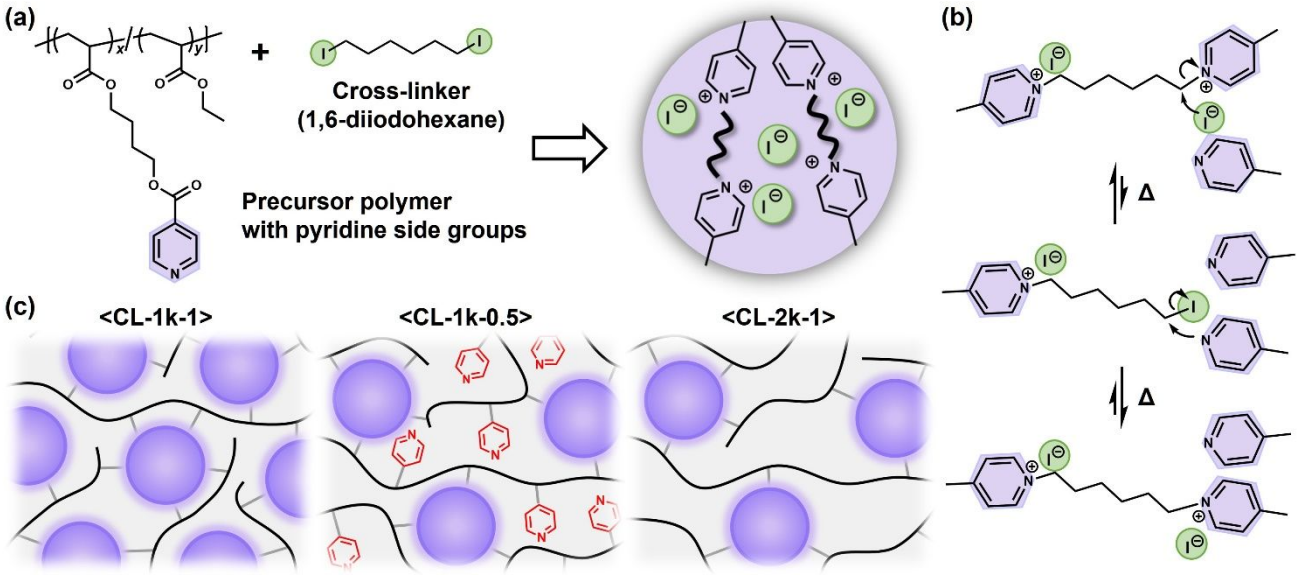

Figure 1. (a) The present material design and trans-*N*-alkylation bond exchange of quaternized pyridine. (c) Schematic of the three samples (see the explanation in the test).

Table 1. Characterization of the precursor polymers

Code	M_n [a]	$Đ$ [a]	n_{EA} / n_{Py} [b]
Py-1k	14800	1.09	105 / 15
Py-2k	13800	1.07	114 / 8

[a]Determined by SEC, according to PMMA standards. [b]The average number of the degree of polymerization for ethyl acrylate units (n_{EA}) and pyridine side group units (n_{Py}).

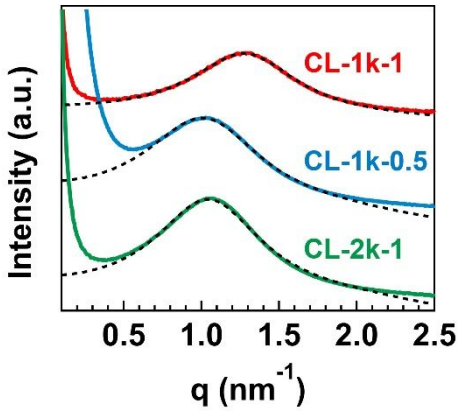

Figure 2. SAXS profiles for the cross-linked samples. The dotted curves are the fitting curves using the Yarusso-Cooper model.

Table 2. Structural features derived from the YC model fitting

Code	R_1 (nm)	R_{CA} (nm)	V_p (nm^3)	K (× 10^{-3})	ND	r (nm)	d (nm)
CL-1k-1	1.28	2.11	80.7	0.44	12.39	2.68	2.80
CL-1k-0.5	1.39	2.56	257.6	1.37	3.88	3.95	5.12
CL-2k-1	1.36	2.52	207.4	1.29	4.82	3.67	4.62

Explanation of all parameters is available in the main text.

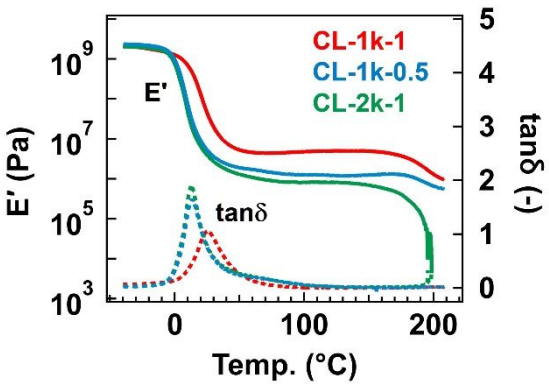

Figure 3. Temperature-ramp rheology data for the cross-linked samples.

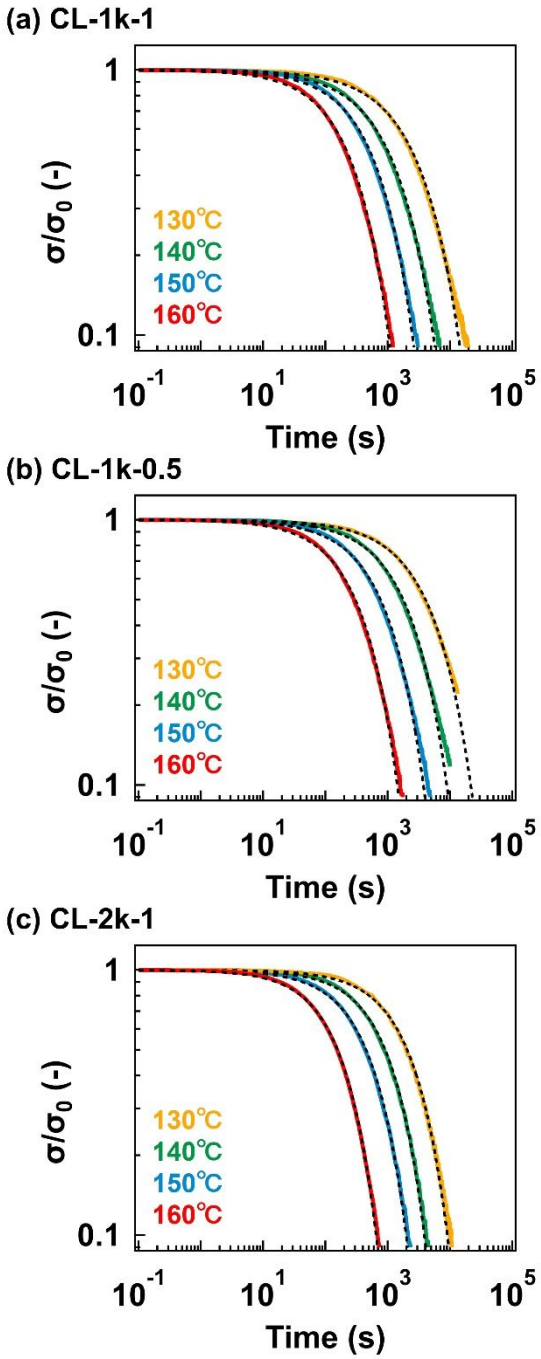

Figure 4. Stress-relaxation spectra at different temperatures for (a) CL-1k-1, (b) CL-1k-0.5, and (c) CL-2k-1. In Y-axis, the stress (σ) is normalized by the initial stress (σ_0).

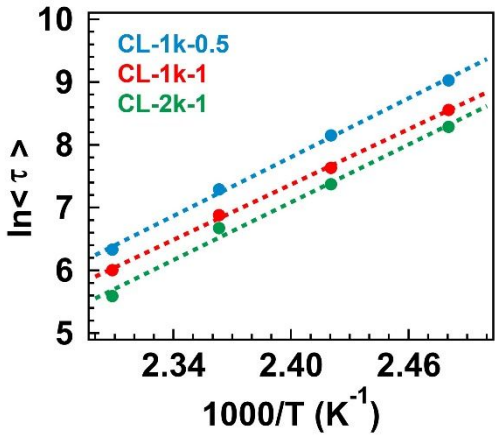

Figure 5. Plots of ln< τ > as a function of inverse temperature for the cross-linked samples. The dotted lines represent approximate straight lines between the points to estimated E_a.

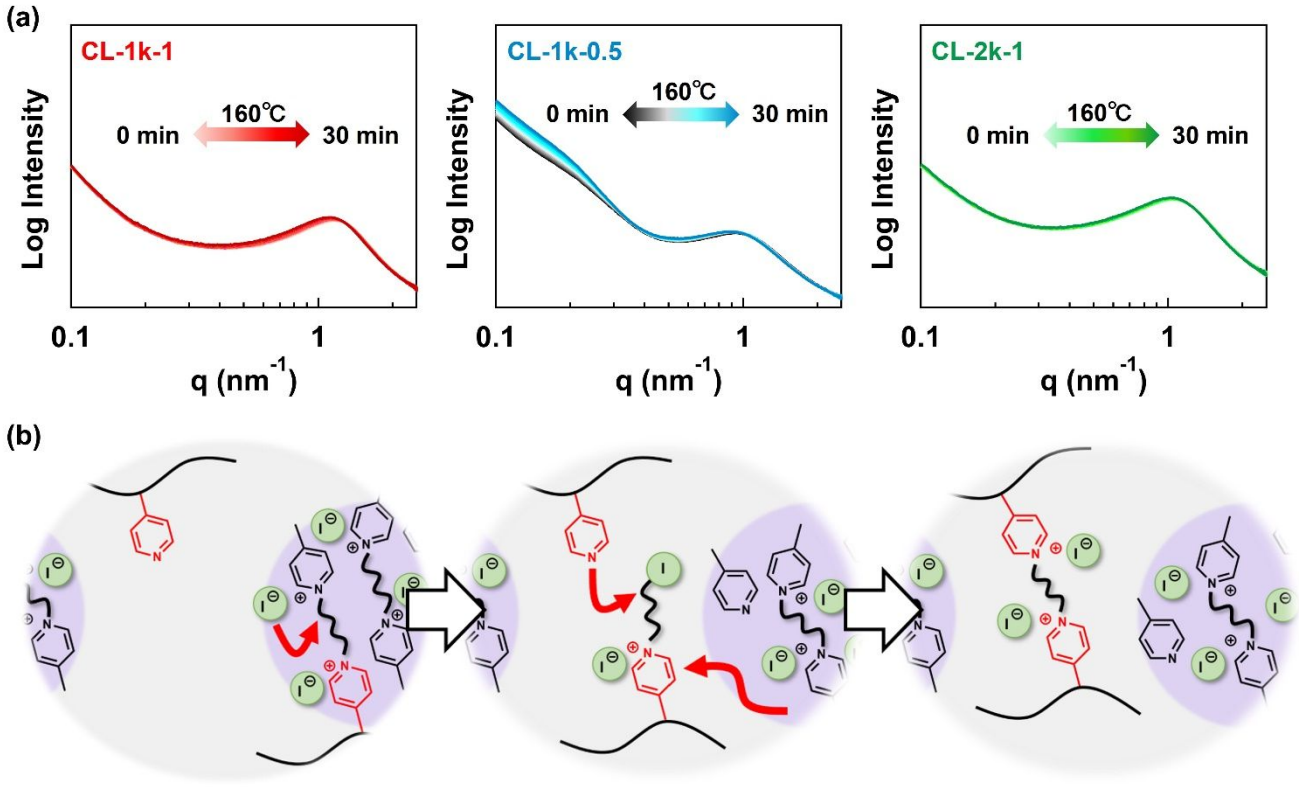

Figure 6. (a) Time-resolved SAXS spectra in heating at 160 °C for three samples. The X-axis is represented with a double-logarithmic scale for clarity. (b) Schematic of the trapping bond exchange phenomenon in CL-1k-0.5.

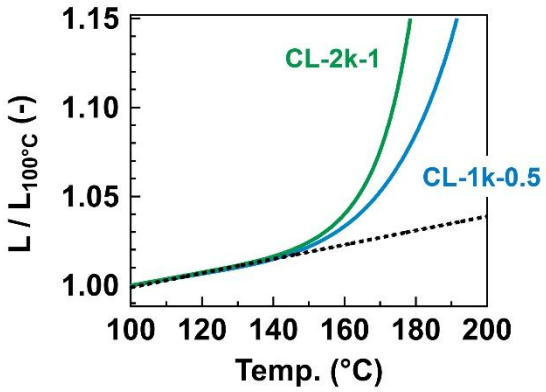

Figure 7. Temperature-ramp creep data. The Y-axis represents the sample length (L) normalized by the length at 100 °C ($L_{100°C}$). The dotted line indicates the approximation straight line extrapolated from low temperature.